Effects of electron-ion temperature equilibration on inertial confinement fusion implosions

Barry Xu and S. X. Hu (□□□)

Phys. Rev. E **84**, 016408 — Published 25 July 2011

DOI: 10.1103/PhysRevE.84.016408

Effects of Electron–Ion Temperature Equilibration on Inertial Confinement Fusion Implosions

Barry Xu and S. X. Hu(胡素兴)*

Laboratory for Laser Energetics, University of Rochester

250 East River Road, Rochester, NY 14623-1299

*E-mail: shu@lle.rochester.edu

The electron–ion temperature relaxation essentially affects both the laser absorption in coronal plasmas and the hot-spot formation in inertial confinement fusion (ICF). It has recently been re-examined for plasma conditions closely relevant to ICF implosions using either classical molecular-dynamics simulations or analytical methods. To explore the electron–ion temperature equilibration effects on ICF implosion performance, we have examined two new Coulomb logarithm models by implementing them into our hydro-codes and carried out hydro-simulations for ICF implosions. Compared to the Lee–More model that is currently used in our standard hydro-codes, the two new models predict substantial differences in laser absorption, coronal temperatures, and neutron yields for ICF implosions on the OMEGA Laser Facility [T. R. Boehly *et al*., Opt. Commun. **133**, 495 (1997)]. Such effects on the triple-picket direct-drive design for the National Ignition Facility (NIF) have also been explored. Based on the validity of the two new models, we have proposed a combined model of the electron–ion temperature-relaxation rate for the overall ICF plasma conditions. The hydro-simulations using the

combined model for OMEGA implosions have shown ~6% more laser absorption, ~6%–15% higher coronal temperatures, and ~10% more neutron yield, when compared to the Lee–More model prediction. It is also noticed that the gain for the NIF direct-drive design can be varied by ~10% among the different electron–ion temperature-relaxation models.

I. INTRODUCTION

In inertial confinement fusion (ICF) implosions, cryogenic (cryo) deuterium–tritium (DT) targets are compressed by laser-driven shocks as well as through spherical convergence.[1] The electrons absorbing the laser energy in the coronal plasma equilibrate their temperature with the ions so that the mass ablation (carried mainly by ions) occurs to drive the shell imploding inward by the so-called "rocket" effect. How quickly the heat flows from the electrons to the ions directly affects both the ablation rate and the laser absorption itself, since the inverse-bremstrahlung process is directly proportional to the Coulomb logarithm–characterizing electron–ion collisions. It is also sensitive to the coronal plasma temperature. On the other hand, the ions can first be heated during the laser-launched shocks propagating through the shell and breaking out into the gas in the target center. The shock-heated ions thermally equilibrate with the electrons both in the shell and in the hot spot. The rate of electron–ion energy transfer may affect the shock propagation through the shell and the hot-spot formation in ICF implosions. For this reason, the electron–ion thermal equilibration rate is very important for ICF simulations and target designs; it has been studied for a variety of plasma conditions over the past decades since the early work of Spitzer.[2]

Different models for improving the original Spitzer formula have been proposed and published in the literature. For example, in 1984, Lee and More[3] considered the quantum degeneracy effects and made modifications to the Spitzer formula for low-temperature plasmas. The Lee–More model has long been used in hydro-codes (e.g., *LILAC*[4] and *DRACO*[5,6] developed at LLE) to simulate ICF implosions. For the inverse-bremsstrahlung absorption of laser energy in coronal plasmas, Skupsky has developed formulas for the Coulomb logarithm of electron–ion collisions under the modified Born approximation.[7] Most recently, the electron–ion energy relaxation has been revisited for density/temperature conditions closely relevant to ICF plasmas, by either classical molecular-dynamics (MD) simulations[8–11] or analytical methods.[12–15] Specifically, Dimonte and Daligault have carried out the *ab initio* classical MD simulations for electron–ion Coulomb plasmas using like charges.[8] By fitting to their MD results, they have formulated the Coulomb logarithm in terms of the coupling parameter g. On the other hand, Brown, Preston, and Singleton (BPS) have recently utilized the dimensional continuation method to work out a formula for the electron–ion energy transfer rate in a wide range of plasma conditions including quantum and coupling effects.[12,13] Although these new models have been proposed for years, to the best of our knowledge there are no studies, to date, on their effects on ICF implosions. In this paper, we have implemented these two new models together with the original Spitzer formula into our hydro-codes and carried out hydro-simulations for cryo-DT implosions on OMEGA[16] as well as for the direct-drive–ignition designs on the National Ignition Facility (NIF).[17] The simulation results indicate that the target performance is sensitive to the electron–ion temperature-relaxation model used. Differences in laser absorption, coronal temperatures,

and neutron yields are significant. Based on the validity of the classical MD model and the BPS model, we suggest the use of a model combined of both for the overall ICF plasma conditions. Such a combined model predicts ~6% more laser absorption, ~6%–15% higher coronal temperatures, and ~10% more neutron yield for OMEGA implosions, when compared to the Lee–More model simulations.

This paper is organized as follows: A brief description of the four different models of electron–ion temperature equilibration and their implementation in the hydro-code *LILAC* is given in Sec. II. The hydro-simulation results for cryo-DT implosions on OMEGA and for the triple-picket, direct-drive NIF design are presented in Sec. III. The combined model of MD fitting and the BPS formula is discussed in Sec. IV, where the implosion performance of the combined model simulation and the standard Lee–More prediction is also compared. A summary is presented in Sec. V.

II. ELECTRON–ION TEMPERATURE-RELAXATION MODELS

In ICF implosions, there are different regions where the temperatures of electrons (T_e) and ions (T_i) are drastically different at given instances. For example, in the coronal regime the electrons absorbing the laser energy get heated first and transfer their energy to ions via collisions; while in the shell and in the hot spot, the shock-heated ions (via complete inelastic collisions) first reach high temperatures, which gradually equilibrate with the electrons as the time goes on. The electron–ion temperature relaxation via collisions is normally described by

$$\frac{\mathrm{d}T_{e/i}}{\mathrm{d}t} = -\nu \times \left(T_e - T_i\right) = -\nu_0 \ln\Lambda \times \left(T_e - T_i\right). \quad (1)$$

For most theories,[2,3,13,18] the electron–ion temperature-relaxation rate involves the same prefactor:

$$\nu_0 = \frac{8}{3} n_{\mathrm{i}} e^4 Z^2 \frac{\sqrt{2\pi m M}}{\left(m k_{\mathrm{B}} T_{\mathrm{i}} + M k_{\mathrm{B}} T_{\mathrm{e}}\right)^{3/2}}, \tag{2}$$

where n_{i} is the ion number density, m and e are the electron mass and charge, Z and M are the ion charge and mass, and k_{B} is the Boltzman constant. (The *cgs* units are used throughout this paper). The Coulomb logarithm $\ln\Lambda$, a unit-less coefficient for the rate of temperature change, characterizes the long-range and short-range electron–ion collisions in plasmas. For different models, the Coulomb logarithm has been approximated to a variety of expressions.

The well-known Spitzer formula[2] for the Coulomb logarithm was introduced to avoid the integral divergence in binary collisions. Specifically, by cutting off the integration to some impact parameters, the Spitzer Coulomb logarithm can be written as

$$\ln\Lambda = \ln\left(\frac{3}{2 Z_{\mathrm{e}} Z_{\mathrm{i}} e^3} \sqrt{\frac{k_{\mathrm{B}}^3 T_{\mathrm{e}}^3}{\pi n_{\mathrm{e}}}} \right), \tag{3}$$

with the electron and ion charges Z_{e} (=1) and Z_{i}. By using the Krook model (under the Lorentz plasma condition) and including the electron-degeneracy effects in low-

temperature plasmas (for example, in the imploding shell of T_e & 50 eV), Lee and More[3] proposed the following formula:

$$\ln \Lambda = \frac{1}{2} \ln \left(1 + b_{\max}^2 / b_{\min}^2 \right) \tag{4}$$

with $b_{\max}$ being the degeneracy-modified Debye–Hückel screening length λ_{DH}, which is defined by

$$\frac{1}{\lambda_{DH}} = \sqrt{\frac{4\pi n_e e^2}{k_B \sqrt{T_e^2 + T_F^2}} + \frac{4\pi n_i Z^2 e^2}{k_B T_i}}, \tag{5}$$

where T_F is the Fermi-degeneracy temperature. The minimum impact parameter $b_{\min}$ is given by the larger of the classical closest-collision distance and the quantum uncertainty-principle limited length:

$$b_{\min} = \max \left(Ze^2 / 3k_B T_e, \hbar / 2\sqrt{3mk_B T_e} \right). \tag{6}$$

It is noted that the Planck constant "h" that originally appeared in Lee and More's paper has been corrected to "$\hbar$".[7] The Lee–More model of Coulomb logarithm has long been used in our hydro-codes *LILAC*[4] and *DRACO*[5,6] for simulations of implosions and planar experiments.[19]

Recently, the electron–ion energy relaxation problem has been revisited for ICF plasma conditions by a number of groups.[8–15] Two new models have formulated explicit expressions for the Coulomb logarithm: One was done by Dimonte and Daligault[8] using the classical MD simulations for electron–ion Coulomb plasmas with like charges. By fitting their MD results, they have come up with the following formula for the Coulomb logarithm in terms of the coupling parameter g:

$$\ln\Lambda = \ln\left(1.0 + 0.7/g\right) \tag{7}$$

with $g = Ze^2/\lambda_D k_B T_e$ and the Debye length $\lambda_D = \sqrt{k_B T_e / 4\pi n_e e^2}$. In contrast to numerical simulations, analytical studies using the dimensional continuation method by Brown, Preston, and Singleton (BPS) have recently resulted in a formula for the electron–ion temperature-equilibration rate in a wide range of plasma conditions including quantum and coupling effects.[12,13] The BPS formula for the Coulomb logarithm is comprised of a main term followed by two correction factors

$$\ln\Lambda_{BPS} = \ln\Lambda_{BPS}^{QM} + \ln\Lambda_{BPS}^{\Delta C} + \ln\Lambda_{BPS}^{FD}. \tag{8}$$

The leading term incorporates quantum effects, while the second term is a correction for the case where the plasma parameters are no longer near the quantum limit; the third term takes into account the many-body electron degeneracy effects when the Fermi–Dirac

statistics becomes relevant. Without considering the small electron–ion mass ratio effects,[13] these terms can be explicitly written as

$$\ln \Lambda_{\mathrm{BPS}}^{\mathrm{QM}} = \frac{1}{2}\left[\ln\left(\frac{8k_{\mathrm{B}}^2 T_{\mathrm{e}}^2}{\hbar^2 \omega_{\mathrm{e}}^2} \right) - \gamma - 1 \right]; \tag{9}$$

$$\ln \Lambda_{\mathrm{BPS}}^{\Delta\mathrm{C}} = -\frac{\epsilon_{\mathrm{H}}}{k_{\mathrm{B}} T_{\mathrm{e}}} \sum_{\mathrm{i}} \frac{Z_{\mathrm{i}}^2 \omega_{\mathrm{i}}^2}{\omega_I^2} \left\{ 1.20205 \times \left[\ln\left(\frac{k_{\mathrm{B}} T_{\mathrm{e}}}{Z_{\mathrm{i}}^2 \epsilon_{\mathrm{H}}} \right) - \gamma \right] + 0.39624 \right\}; \tag{10}$$

$$\ln \Lambda_{\mathrm{BPS}}^{\mathrm{FD}} = \frac{n_{\mathrm{e}} \lambda_{\mathrm{e}}^3}{2} \left\{ -\frac{1}{2}\left(1 - \frac{1}{2^{3/2}} \right) \times \left[\ln\left(\frac{8k_{\mathrm{B}}^2 T_{\mathrm{e}}^2}{\hbar^2 \omega_{\mathrm{e}}^2} \right) - \gamma - 1 \right] + \left(\frac{\ln 2}{2} + \frac{1}{2^{5/2}} \right) \right\} \tag{11}$$

with the binding energy ϵ_{H} of the hydrogen atom, the Euler constant $\gamma \approx 0.57721$, the electron-plasma frequency $\omega_{\mathrm{e}} = \sqrt{4\pi n_{\mathrm{e}} e^2 / m}$, and the ion-plasma frequency ω_{i} for each ion species and the average ion frequency $\omega_I = \sqrt{\sum_{\mathrm{i}} \omega_{\mathrm{i}}^2}$, as well as the electron thermal wavelength $\lambda_{\mathrm{e}} = \hbar \sqrt{2\pi / m k_{\mathrm{B}} T_{\mathrm{e}}}$. By implementing these formulas into our 1-D hydro-code *LILAC*, we have examined how our ICF implosion performance is affected by the choice of Coulomb logarithm model. By analyzing the validity of each model, we suggest a combined model that incorporates the BPS formula for the high-density shell and the MD fitting formula for the corona and hot-spot regimes. Compared to the standard (Lee–More) model prediction, such a combined model has shown ~6% more laser absorption,

~6–15% higher coronal temperatures, and ~10% greater neutron yield for cryogenic-DT implosions on OMEGA.

To compare the different model predictions for the Coulomb logarithm, we have plotted the value of lnΛ as a function of electron density in Fig. 1 for typical ICF plasma conditions: (a) T_e = 5 keV and T_i = 10 keV (during shock convergence in the "hot spot" of NIF implosions), (b) T_e = 2.5 keV and T_i = 5 keV (during shock convergence in the hot spot of OMEGA implosions), (c) T_e = 2.0 keV and T_i = 1.0 keV (typical "corona" condition on OMEGA implosions), and (d) T_e = 50 eV and T_i = 100 eV (imploding-shell condition of OMEGA targets), respectively. In the panels of Fig. 1, the black dotted lines represent the Spitzer model, while the blue long-dashed lines represent the Lee–More model currently used in our hydro-codes. The two new models "MD" [Eq. (7)] and "BPS" [Eq. (8)] are depicted by the red solid line and the green dashed line, respectively. Overall, the Spitzer model gives the highest limit for all cases. For the hot-spot conditions on both OMEGA and NIF, the two new models are close to the Lee–More model and the difference is within ~10%, as shown by Figs. 1(a) and 1(b). The MD results, which were claimed in good agreement with previous BPS formula for low T_e, are higher than the BPS results for temperatures larger than ~1 keV. Figure 1(c) shows that at the typical coronal temperature of OMEGA implosions, the BPS model gives very close results in comparison with the Lee–More model's prediction near the critical-density regime (n_e ~ $9.1 \times 10^{21}/\text{cm}^3$) of OMEGA's UV laser ($\lambda$ = 0.351 μm). The Spitzer and MD results are ~5-15% higher than the other two. Such a difference in lnΛ would affect the laser absorption in the corona, which will subsequently have a consequence on target performance. Inside the imploding DT shell, the electron/ion temperature is below

~100 eV during the implosion (before stagnation), where the DT plasma is moderately coupled and partially degenerated.[20] Therefore, one would expect the quantum and many-body effects to begin to be important. For such conditions, Fig. 1(d) shows that the BPS model gives different results from the Spitzer and the Lee–More models, while the classical MD result was counter-intuitively in agreement with the BPS result at such low temperature regime [similar to what was shown in Ref. (8)]. The BPS result indicates an increase at very high density, which manifests the degeneracy effects since the plasma temperature is well below the Fermi temperature.

III. HYDRO-SIMULATION RESULTS AND DISCUSSIONS

The different electron-ion temperature-equilibration models discussed above have been implemented into our 1-D hydro-code *LILAC*,[4] which was used to simulate the cryo-DT implosions on OMEGA as well as the direct-drive NIF design. On OMEGA the triple picket plus a step main pulse shape has been applied to implode cryo-DT targets,[21–22] [see Fig. 2(a)]. The shocks launched by the pickets precisely place the imploding shell in an appropriate adiabat ($\alpha \sim 2$), and a high compression of $\langle \rho R \rangle \sim 300$ mg/cm^2 has been reached in cryo-DT implosions on OMEGA.[21–23] The typical OMEGA target consists of a 10-μm deuterated plastic (CD) shell, ~65 μm of DT ice, and about 3 atm of DT gas in the center. The *LILAC* simulation results (with the standard flux limiter $f = 0.06$) are plotted in Figs. 2 and 3. The laser absorptions predicted by different Coulomb logarithm models are shown in Fig. 2(b). We see that the Lee–More model (used in the standard *LILAC*) and the BPS formula predict the lowest laser absorption, since Fig. 1 has indicated that these two models give smaller lnΛ in the plasma corona

[see Fig. 1(c)]. It is noted that the inverse bremstrahlung absorption is linearly proportional to the Coulomb logarithm. At the end of the laser pulse, the classical MD result is close to the Spitzer result. The absorption difference between the models can be as high as ≥6%. The corresponding compression ρR history and the neutron yield are shown in Figs. 3(a) and 3(b), respectively. Compared to the Lee–More model and the BPS formula, the MD and Spitzer models give slightly higher ρR and the peak ρR shifts slightly early, which is consistent with the greater absorption seen in Fig. 2(b). The neutron yields plotted in Fig. 3(b) are 7.54×10^{13} (Lee–More), 1.02×10^{14} (MD), 6.73×10^{13} (BPS), and 1.25×10^{14} (Spitzer), respectively. The yield variation between the Lee–More model and the two new models (MD and BPS) is ~30% and ~10% respectively.

Similar *LILAC* simulations for the direct-drive NIF design have also been performed, and simulation results are presented in Figs. 4 and 5. Figure 4(a) shows the NIF pulse design, which will be used for imploding the NIF-scale DT targets (~37-μm CD with ~150-μm of DT ice and a target diameter ϕ =3.374 mm). For NIF implosions, the plasma density scale-length is long (L ~ 300–400 μm), so that the laser absorption is ~95% in all four Coulomb logarithm models. The Lee–More and BPS models still predict the lowest absorption, especially during the first picket [see Fig. 4(b)]. The compression ρR and neutron yield are correspondingly shown in Figs. 5(a) and 5(b), respectively. Depending on the slightly different shock dynamics, Fig. 5(a) indicates a small compression difference among these models. From the neutron yield illustrated in Fig. 5(b), we find the final target gains are ~10% different among the different electron–ion temperature-equilibration models: 45.5 (Lee–More), 48.2 (Spitzer), 44.2 (BPS), and 49.5 (MD).

IV. THE COMBINED MD–BPS MODEL

Since the coronal/hot-spot electron temperatures are above ~2 keV for ICF implosions where the density is low, the classical MD simulations, which were performed in an *ab initio* fashion, would better characterize the classical electron–ion thermal equilibrium process there. While in the low-adiabat shell, the plasmas are moderately coupled and partially degenerated[20] so that the BPS formula, which has incorporated these quantum effects, should be suitable for the shell conditions. Therefore, we have suggested a combined model in which the MD result is used for plasma densities less than the critical density, while the BPS formula applies for the dense shell. Namely, the MD result is used for the domain in which the plasma coupling parameter $g < 0.1$, while the BPS formula applies to the regime of $g \geq 0.1$. Employing this combined model, we have simulated the OMEGA implosion studied in Figs. 2 and 3 and the NIF design discussed in Figs. 4 and 5. The simulation results are presented in Figs. 6-10. For the OMEGA implosion, we plotted the laser absorption predicted by the combined model in comparison with the Lee–More model in Fig. 6(a). Again, the combined model gives ~6% higher absorption than the Lee–More prediction. Consequently, the combined model results in ~10% more neutron yield than the standard *LILAC* (Lee–More) case. It is also interesting to see that the coronal electron and ion temperatures are quite different in the simulations using the combined model versus the Lee–More model. As an example, we plotted in Fig. 7 the coronal temperatures at $t = 3.0$ ns as a function of radius. Figure 7 indicates that the combined model predicts ~6% hotter electron temperature [Fig. 7(a)] and ~15% hotter ion temperature [Fig. 7(b)] when compared to the Lee–More case. The

large temperature differences should be measurable with Thompson scattering,[24,25] which is being planned for OMEGA implosion experiments. Such measurements are expected to differentiate between the electron–ion temperature-equalibration models discussed here.

Similar simulations have also been performed for the NIF-design pulse shape [Fig. 4(a)]. Again, the combined model predicts slightly higher laser absorption and more neutron yield than the Lee–More case, as shown in Fig. 8. Similar to the OMEGA implosion, Fig. 9 indicates that the coronal temperatures are ~5%–10% hotter in the combined-model prediction. The final target gain given by the combined model is ~43.6, which is ~5% lower than the Lee–More model prediction.

V. SUMMARY

In summary, we have investigated the electron–ion temperature-equilibration effects on the cryo-DT implosions on OMEGA and on the NIF direct-drive design. Different electron–ion Coulomb-logarithm models have been examined and implemented into our hydro-codes. Hydro-simulations show that the OMEGA implosion performance is sensitive to the electron–ion temperature-equilibration models since the inverse bremstrahlung laser absorption is closely related to the electron–ion Coulomb logarithm and the coronal temperatures. A combined model of the electron–ion temperature-relaxation rate, which incorporates the classical MD result and the BPS formula, has been proposed for the overall ICF plasma conditions. The hydro-simulations using the combined model for OMEGA implosions have shown ~6% more laser absorption, ~6%–15% higher coronal temperatures, and ~10% more neutron yield, when compared to the

Lee–More model (used in the standard *LILAC*) prediction. It has also shown that the gain for the NIF direct-drive design can be varied by ~10% among the different electron–ion temperature-relaxation models.

ACKNOWLEDGMENT

This work was supported by the U.S. Department of Energy (DOE) Office of Inertial Confinement Fusion under Cooperative Agreement No. DE-FC52-08NA28302, the University of Rochester, and the New York State Energy Research and Development Authority.

REFERENCES

1. S. Atzeni and J. Meyer-ter-Vehn, *The Physics of Inertial Fusion: Beam Plasma Interaction, Hydrodynamics, Hot Dense Matter*, International Series of Monographs on Physics (Clarendon Press, Oxford, 2004); J. D. Lindl, *Inertial Confinement Fusion: The Quest for Ignition and Energy Gain Using Indirect Drive* (Springer-Verlag, New York, 1998).
2. L. Spitzer, *Physics of Fully Ionized Gases*, 2nd rev. ed., Interscience Tracts on Physics and Astronomy (Interscience, New York, 1962).
3. Y. T. Lee and R. M. More, Phys. Fluids **27**, 1273 (1984).
4. J. Delettrez, R. Epstein, M. C. Richardson, P. A. Jaanimagi, and B. L. Henke, Phys. Rev. A **36**, 3926 (1987).
5. P. B. Radha, T. J. B. Collins, J. A. Delettrez, Y. Elbaz, R. Epstein, V. Yu. Glebov, V. N. Goncharov, R. L. Keck, J. P. Knauer, J. A. Marozas, F. J. Marshall, R. L. McCrory, P. W. McKenty, D. D. Meyerhofer, S. P. Regan, T. C. Sangster, W. Seka, D. Shvarts, S. Skupsky, Y. Srebro, and C. Stoeckl, Phys. Plasmas **12**, 056307 (2005).
6. S. X. Hu, P. B. Radha, J. A. Marozas, R. Betti, T. J. B. Collins, R. S. Craxton, J. A. Delettrez, D. H. Edgell, R. Epstein, V. N. Goncharov, I. V. Igumenshchev, F. J. Marshall, R. L. McCrory, D. D. Meyerhofer, S. P. Regan, T. C. Sangster, S. Skupsky, V. A. Smalyuk, Y. Elbaz, and D. Shvarts, Phys. Plasmas **16**, 112706 (2009).
7. S. Skupsky, Phys. Rev. A **36**, 5701 (1987).
8. G. Dimonte and J. Daligault, Phys. Rev. Lett. **101**, 135001 (2008).

9. B. Jeon, M. Foster, J. Colgan, G. Csanak, J. D. Kress, L. A. Collins, and N. Grønbech-Jensen, Phys. Rev. E **78**, 036403 (2008).

10. J. N. Glosli, F. R. Graziani, R. M. More, M. S. Murillo, F. H. Streitz, M. P. Surh, L. X. Benedict, S. Hau-Riege, A. B. Langdon, and R. A. London, Phys. Rev. E **78**, 025401 (R) (2008).

11. L. X. Benedict, J. N. Glosli, D. F. Richards, F. H. Streitz, S. P. Hau-Riege, R. A. London, F. R. Graziani, M. S. Murillo, and J. F. Benage, Phys. Rev. Lett. **102**, 205004 (2009).

12. L. S. Brown, D. L. Preston, and R. L. Singleton, Jr, Phys. Rep. **410**, 237 (2005).

13. L. S. Brown and R. L. Singleton Phys. Rev. E **79**, 066407 (2009).

14. M. S. Murillo and M. W. C. Dharma-wardana, Phys. Rev. Lett. **100**, 205005 (2008).

15. M. W. C. Dharma-wardana, Phys. Rev. Lett. **101**, 035002 (2008).

16. T. R. Boehly, D. L. Brown, R. S. Craxton, R. L. Keck, J. P. Knauer, J. H. Kelly, T. J. Kessler, S. A. Kumpan, S. J. Loucks, S. A. Letzring, F. J. Marshall, R. L. McCrory, S. F. B. Morse, W. Seka, J. M. Soures, and C. P. Verdon, Opt. Commun. **133**, 495 (1997).

17. E. M. Campbell and W. J. Hogan, Plasma Phys. Control. Fusion **41**, B39 (1999).

18. R. S. Cohen and L. Spitzer, Jr., Phys. Rev. **80**, 230 (1950); W. B. Thompson and J. Hubbard, Rev. Mod. Phys. **32**, 714 (1960).

19. V. A. Smalyuk, S. X. Hu, V. N. Goncharov, D. D. Meyerhofer, T. C. Sangster, D. Shvarts, C. Stoeckl, B. Yaakobi, J. A. Frenje, and R. D. Petrasso, Phys. Rev. Lett. **101**, 025002 (2008); V. A. Smalyuk, S. X. Hu, V. N. Goncharov, D. D.

Meyerhofer, T. C. Sangster, C. Stoeckl, and B. Yaakobi, Phys. Plasmas **15**, 082703 (2008); S. X. Hu, V. A. Smalyuk, V. N. Goncharov, J. P. Knauer, P. B. Radha, I. V. Igumenshchev, J. A. Marozas, C. Stoeckl, B. Yaakobi, D. Shvarts, T. C. Sangster, P. W. McKenty, D. D. Meyerhofer, S. Skupsky, and R. L. McCrory, Phys. Rev. Lett. **100**, 185003 (2008); S. X. Hu, V. A. Smalyuk, V. N. Goncharov, S. Skupsky, T. C. Sangster, D. D. Meyerhofer, and D. Shvarts, Phys. Rev. Lett. **101**, 055002 (2008); V. A. Smalyuk, S. X. Hu, J. D. Hager, J. A. Delettrez, D. D. Meyerhofer, T. C. Sangster, and D. Shvarts, Phys. Rev. Lett. **103**, 105001 (2009); *ibid.*, Phys. Plasmas **16**, 112701 (2009).

20. S. X. Hu, B. Militzer, V. N. Goncharov, and S. Skupsky, Phys. Rev. Lett. **104**, 235003 (2010).

21. V. N. Goncharov, T. C. Sangster, T. R. Boehly, S. X. Hu, I. V. Igumenshchev, F. J. Marshall, R. L. McCrory, D. D. Meyerhofer, P. B. Radha, W. Seka, S. Skupsky, C. Stoeckl, D. T. Casey, J. A. Frenje, and R. D. Petrasso, Phys. Rev. Lett. **104**, 165001 (2010).

22. T. C. Sangster, V. N. Goncharov, R. Betti, T. R. Boehly, D. T. Casey, T. J. B. Collins, R. S. Craxton, J. A. Delettrez, D. H. Edgell, R. Epstein, K. A. Fletcher, J. A. Frenje, V. Yu. Glebov, D. R. Harding, S. X. Hu, I. V. Igumenshchev, J. P. Knauer, S. J. Loucks, C. K. Li, J. A. Marozas, F. J. Marshall, R. L. McCrory, P. W. McKenty, D. D. Meyerhofer, P. M. Nilson, S. P. Padalino, R. D. Petrasso, P. B. Radha, S. P. Regan, F. H. Seguin, W. Seka, R. W. Short, D. Shvarts, S. Skupsky, V. A. Smalyuk, J. M. Soures, C. Stoeckl, W. Theobald, and B. Yaakobi, Phys. Plasmas **17**, 056312 (2010).

23. S. X. Hu, V. N. Goncharov, P. B. Radha, J. A. Marozas, S. Skupsky, T. R. Boehly, T. C. Sangster, D. D. Meyerhofer, and R. L. McCrory, Phys. Plasmas **17**, 102706 (2010).

24. D. H. Froula, J. S. Ross, B. B. Pollock, P. Davis, A. N. James, L. Divol, M. J. Edwards, A. A. Offenberger, D. Price, R. P. J. Town, G. R. Tynan, and S. H. Glenzer, Phys. Rev. Lett. **98**, 135001 (2007).

25. D. H. Froula, J. S. Ross, L. Divol, and S. H. Glenzer, Rev. Sci. Instrum. **77**, 10E522 (2006).

FIGURE CAPTIONS

FIG. 1. (Color online) The Coulomb logarithm as a function of electron density for the four different electron–ion temperature-relaxation models, at different ICF plasma temperatures: (a) T_e = 5 keV and T_i = 10 keV ("hot-spot" condition on NIF); (b) T_e = 2.5 keV and T_i = 5 keV (hot-spot condition on OMEGA); (c) T_e = 2.0 keV and T_i = 1.0 keV ("corona" condition on OMEGA); and (d) T_e = 50 eV and T_i = 100 eV (shell condition).

FIG. 2. (Color online) (a) The laser pulse shape used for cryo-DT implosions on OMEGA; (b) the time-dependent laser absorptions predicted by the four different electron-ion temperature-relaxation models.

FIG. 3. (Color online) The areal density ρR (a) and neutron yield (b) predicted by the four different electron–ion temperature-relaxation models.

FIG. 4. (Color online) (a) The laser pulse shape designed for direct-drive ignition on the NIF; (b) the corresponding laser absorptions predicted by the four different electron–ion temperature-relaxation models.

FIG. 5. (Color online) The areal density ρR (a) and neutron yield (b) predicted for the NIF design by the four different electron–ion temperature-relaxation models.

FIG. 6. (Color online) (a) The laser-absorption comparison between the Lee–More model (long dashed) and the MD–BPS combined model (solid); (b) the neutron yield history predicted by the two models.

FIG. 7. (Color online) The spatial profile of (a) the electron and (b) the ion temperatures for the cryogenic-DT OMEGA shot examined in Fig. 6, at t = 3.0 ns during the main pulse.

FIG. 8. (Color online) (a) The laser-absorption comparison between the Lee–More model (long dashed) and the MD–BPS combined model (solid) for the triple-picket NIF design; (b) the corresponding neutron yield history predicted by the two models.

FIG. 9. (Color online) The spatial profile of (a) the electron and (b) the ion temperatures for the NIF design examined in Fig. 8, at t = 8.0 ns during the main pulse.

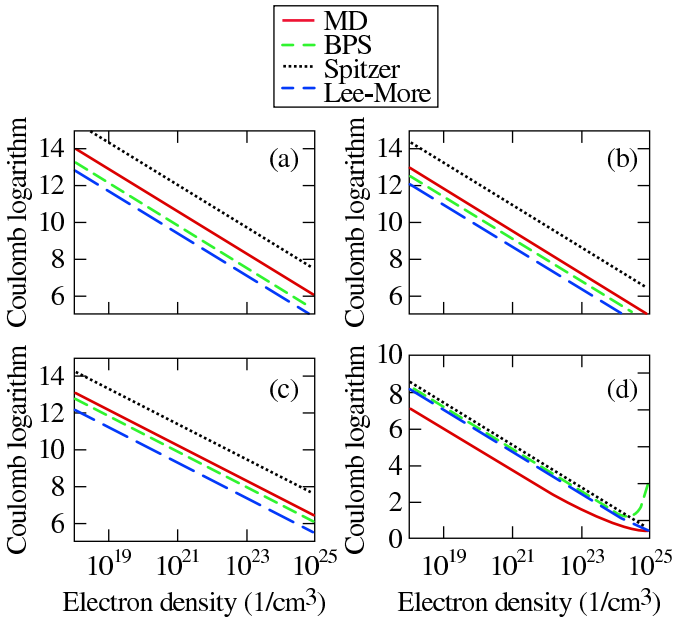

Figure 1 ED10756 10JUN2011

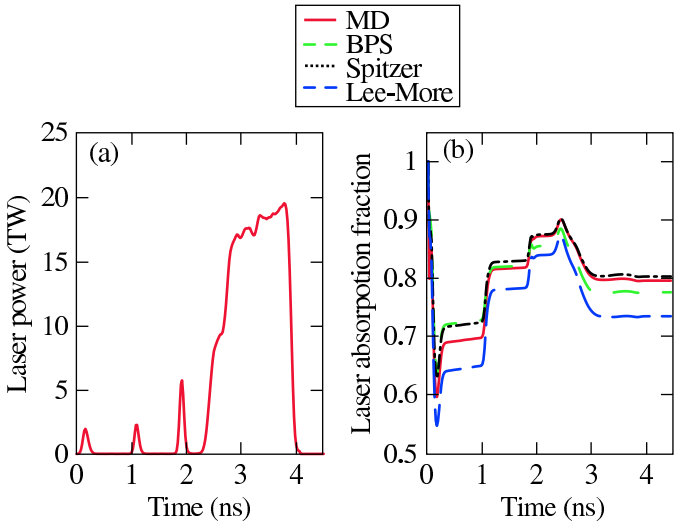

Figure 2 ED10756 10JUN2011

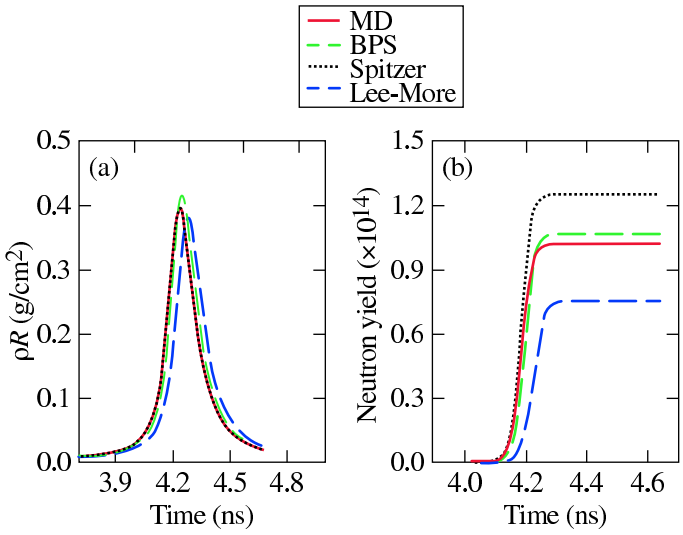

Figure 3 ED10756 10JUN2011

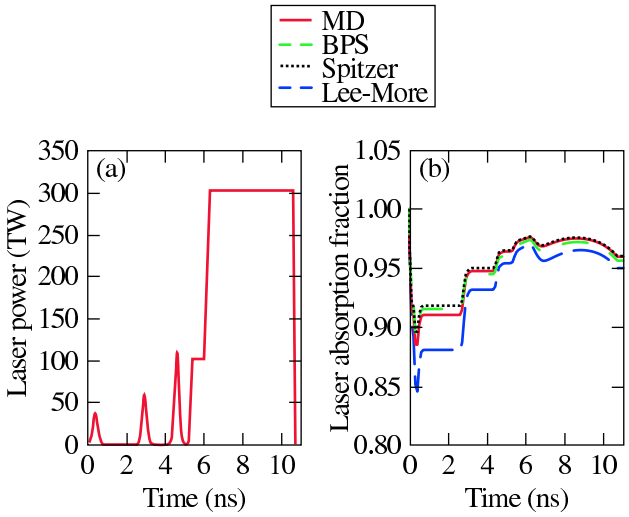

Figure 4 ED10756 10JUN2011

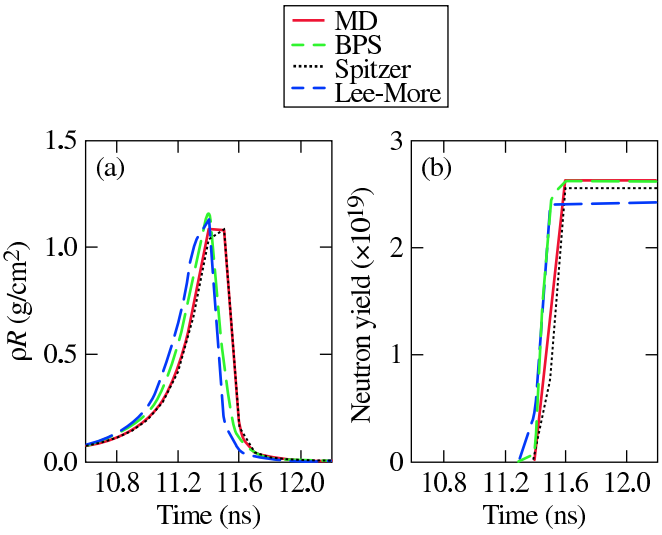

Figure 5 ED10756 10JUN2011

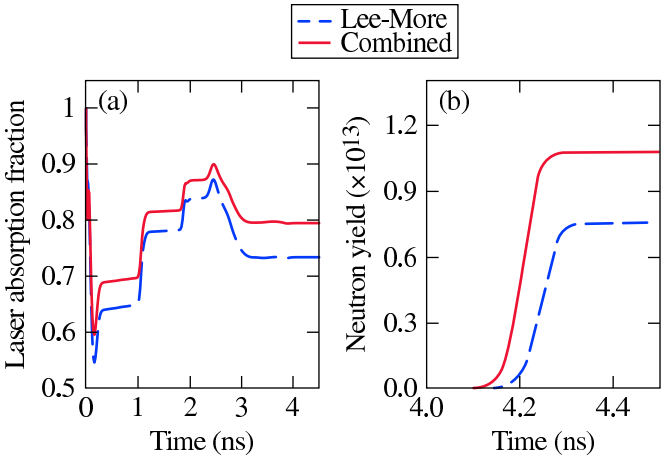

Figure 6 ED10756 10JUN2011

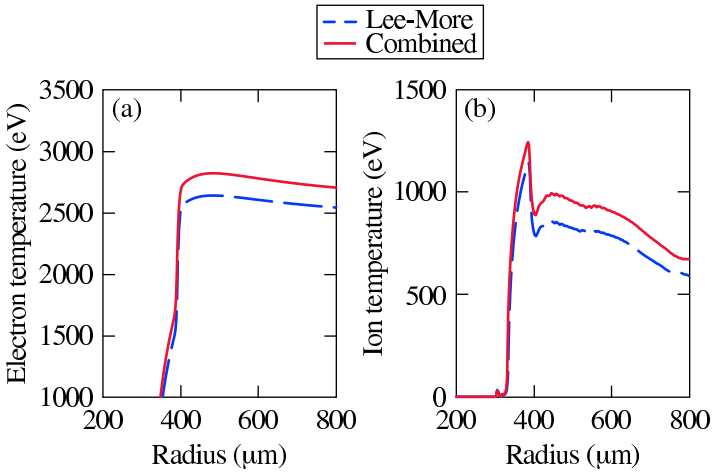

Figure 7 ED10756 10JUN2011

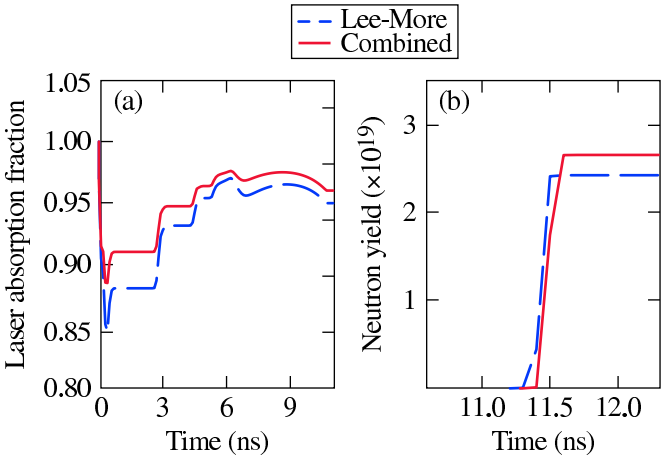

Figure 8 ED10756 10JUN2011

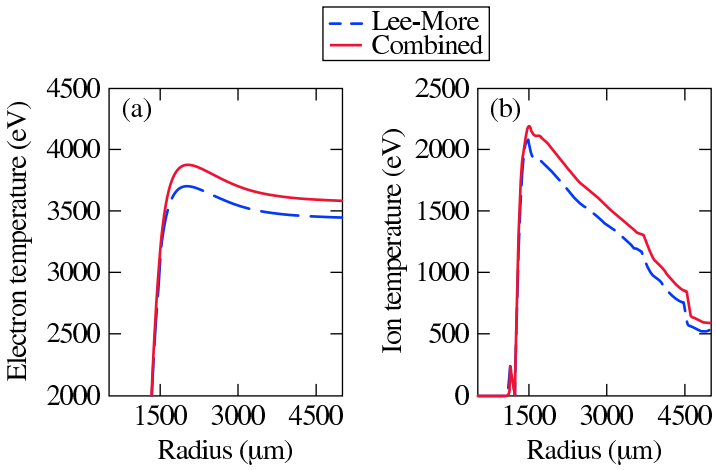

Figure 9 ED10756 10JUN2011